

# Boundary conditions for the electronic structure of finite-extent, embedded semiconductor nanostructures

Seungwon Lee, Fabiano Oyafuso, Paul von Allmen, and Gerhard Klimeck

*Jet Propulsion Laboratory, California Institute of Technology, Pasadena, California 91109*

(Dated: May 28, 2018)

## Abstract

The modeling of finite-extent semiconductor nanostructures that are embedded in a host material requires a proper boundary treatment for a finite simulation domain. For the study of a self-assembled InAs dot embedded in GaAs, three kinds of boundary conditions are examined within the empirical tight-binding model: (i) the periodic boundary condition, (ii) raising the orbital energies of surface atoms, and (iii) raising the energies of dangling bonds at the surface. The periodic boundary condition requires a smooth boundary and consequently a larger GaAs buffer than the two non-periodic boundary conditions. Between the non-periodic conditions, the dangling-bond energy shift is more numerically efficient than the orbital-energy shift, in terms of the elimination of non-physical surface states in the energy region of interest for interior states. A dangling-bond energy shift larger than 5 eV efficiently eliminates all of the surface states and leads to interior states that are highly insensitive to the choice of the energy shift.

## I. INTRODUCTION

The representation of a semiconductor heterostructure by an atomistic model ultimately requires the introduction of a limited simulation domain, of which the surface needs to be treated with a specific boundary condition (BC). If the surface of the simulation domain is selected far enough from the central feature of interest, periodic BCs can be used and the simulation domain is effectively repeated infinitely. However, for electronic devices with non-periodic external potentials or for structures with irregular surfaces, the periodic BCs are not a natural choice. If the simulation-domain surface is within the material bulk region, a truly open BC or perfectly absorbing BC would be the best solution, as it does not introduce an artificial periodicity and would enable the simulation of carrier injection or transport.[1, 2] However such a BC requires the inversion of a full matrix that is of the order of the number of atoms on the open surface. Therefore, the open BC can only be applied to relatively small open surfaces.

Another choice in representing a finite simulation domain is the abrupt termination of the simulation domain with a hard-wall BC. Such abrupt termination in the atomistic basis set results in the creation of dangling bonds. The dangling bonds will form surface states (of the order of the number of exposed atoms), that typically cover a broad energy range and often litter the central energy region of the fundamental band gap. The separation of the artificially introduced surface states from the desired centrally confined states is numerically expensive, as the computation time and required memory increase with the number of computed eigenvalues and eigenvectors and as the separation would demand the computation of eigenvectors. Many relevant quantum dot calculations only require the computation of eigenvalues,[3] while the computation of the eigenvectors at least doubles the computation time and the required memory scales with the number of computed eigenvectors. To address the problem of artificially introduced surface states, this paper examines two modified hard-wall BCs and discusses their merits relative to each other and to the more standard periodic BC.

Typical quantum-dot and heterostructure devices are based on the concept of confining electron and hole states into a spatial domain. The confinement is typically achieved by surrounding a core semiconductor by a buffer semiconductor of larger band gap. The practical question now arises of how large of a buffer region must be included in the explicit

simulation domain. In systems of strain-induced self-assembled quantum dots the strain fields may extend out from the central device region for tens of nanometers,[4] while the quantum states of interest extend only over a few atomic monolayers into the buffer. The lattice distortion due to strain must therefore be computed in a large simulation domain, while the desired quantum confined states may only need to be computed in a relatively small simulation domain. The hard wall BCs considered in this paper enable the strain and electronic structure simulations to be performed with two different simulation domains. This paper demonstrates that the inclusion of a realistically large buffer is essential to capture the effects of strain, while the subsequent electronic structure calculation can then be performed with a significantly smaller, strain distorted simulation domain which resolves the confined quantum states of interest. The reduction of the simulation domain for the electronic structure calculation substantially lessens the computational requirements since the dimension of the Hamiltonian grows linearly with the number of atoms included in the model.

The proper BC for a reduced buffer should efficiently eliminate all non-physical surface states and at the same time should minimally affect physical interior states. In previous work, two types of BC have been considered for the atomistic modeling of embedded nanostructures.[4, 5] In the first BC, the orbital energy of the surface atoms is raised by a specific amount.[4] The value of energy shift is determined empirically by requiring that no state resides in the energy gap.[4] We will show that this method is unpredictable and numerically less efficient than the new BC proposed in this work. The second BC found in the literature is the periodic BC with a truncated buffer.[5] We also find this method inefficient in eliminating spurious states formed in the energy gap region as it requires either a relatively larger buffer or an unphysical, empirical adjustment to atomic positions near the boundary for a small buffer. In the present work, we propose a new BC that is to raise the energy of dangling bonds. We compare the proposed BC with the two previously employed BCs and demonstrate the efficiency and reliability of the new BC. The three boundary conditions are applied to the study of the electronic structure of a self-assembled InAs quantum dot embedded in a GaAs buffer in the framework of the empirical tight-binding model. The efficiency and reliability of the BCs are measured by the elimination of non-physical surface states, the number of iterations in the Lanczos eigenvalue solver, and the reduction of the buffer size required for interior-state energy convergence.

## II. BOUNDARY CONDITIONS

The first boundary condition (BC I) considered is to raise the orbital energies of surface atoms. This method discourages electrons from populating the surface-atom orbitals. However, this treatment does not differentiate details of the surface atoms such as the number and direction of their dangling bonds. As a refinement, a second boundary condition (BC II) is introduced: raising the energy of the dangling bond for the surface atoms. Within this method, the connected-bond energy of the surface atoms is kept unchanged and hence there is no extra penalty for electrons to occupy the connected bonds of surface atoms. Since the motivation of the surface energy shift in BC I and II is to remove non-physical surface states from the energy region of interest, lowering the surface energies will have the same outcome as raising the surface energies.

Both BC I and II are closed boundary conditions as opposed to a periodic condition that is the third boundary condition (BC III) considered in this work. In principle, this boundary condition is applicable only if the system is composed of a unit cell periodically repeated. However, the periodic boundary condition is widely used not only for periodic systems but also for systems with non-periodic perturbations such as alloy disorder, defects, impurities, and even surfaces. For systems with such non-periodic perturbations, the unit cell known as the supercell should be large enough to accommodate the non-periodic perturbations. In nanostructure modeling, the supercell can be as large as the whole size of the nanostructures. For instance, the nanostructure composed of a quantum dot and a surrounding buffer has no inherent periodicity, with a long-ranged strain field that extends up to tens of nanometers.[4] The periodic boundary condition is therefore examined for its appropriateness and efficiency in modeling these nanostructures.

These three boundary conditions are implemented in the framework of the orthogonal nearest-neighbor tight-binding model. In this model, the effective Hamiltonian is expressed as the sum of the couplings between atomic basis orbitals  $|i, \gamma\rangle$ :

$$H_0 = \sum_{i\gamma} \epsilon_\gamma |i, \gamma\rangle \langle i, \gamma| + \sum_{i \neq i', \gamma \neq \gamma'} t_{ii'\gamma\gamma'} |i, \gamma\rangle \langle i', \gamma'|, \quad (1)$$

where indices  $i$  and  $\gamma$  denote an atomic site and an orbital type. Parameter  $\epsilon$  represents the energy of the basis orbital, and  $t$  accounts for the coupling between basis orbitals centered at nearest-neighbor atomic sites.

In BC I, the Hamiltonian block matrix for a surface atom with basis set  $\{|s\rangle, |p_x\rangle, |p_y\rangle, |p_z\rangle\}$  is given by

$$\begin{bmatrix} \epsilon_s + \delta_s & 0 & 0 & 0 \\ 0 & \epsilon_p + \delta_p & 0 & 0 \\ 0 & 0 & \epsilon_p + \delta_p & 0 \\ 0 & 0 & 0 & \epsilon_p + \delta_p \end{bmatrix}, \quad (2)$$

where  $\delta_\gamma$  is the energy shift for the orbital  $\gamma$  on a surface atom. A different energy shift can be chosen for each basis orbital.

For BC II, the basis set of the Hamiltonian is first changed from set  $\{|s\rangle, |p_x\rangle, |p_y\rangle, |p_z\rangle\}$  to the set of  $sp^3$  hybridized orbitals that are aligned along the bond directions. In the zinc-blende structure, the  $sp^3$  hybridized orbitals are given by[6]

$$\begin{aligned} |sp_a^3\rangle &= \frac{1}{2}(|s\rangle + |p_x\rangle + |p_y\rangle + |p_z\rangle), \\ |sp_b^3\rangle &= \frac{1}{2}(|s\rangle + |p_x\rangle - |p_y\rangle - |p_z\rangle), \\ |sp_c^3\rangle &= \frac{1}{2}(|s\rangle - |p_x\rangle + |p_y\rangle - |p_z\rangle), \\ |sp_d^3\rangle &= \frac{1}{2}(|s\rangle - |p_x\rangle - |p_y\rangle + |p_z\rangle). \end{aligned} \quad (3)$$

The energy of a hybridized orbital is raised by  $\delta_{sp^3}$  if the orbital is along the dangling bond direction. For instance, if the surface atom has dangling bonds along  $|sp_a^3\rangle$  and  $|sp_c^3\rangle$  directions, the Hamiltonian block matrix for the surface atom in the basis set  $\{|sp_a^3\rangle, |sp_b^3\rangle, |sp_c^3\rangle, |sp_d^3\rangle\}$  is given by

$$\begin{bmatrix} a + \delta_{sp^3} & b & b & b \\ b & a & b & b \\ b & b & a + \delta_{sp^3} & b \\ b & b & b & a \end{bmatrix}, \quad (4)$$

where  $a = \epsilon_s/4 + 3\epsilon_p/4$  and  $b = \epsilon_s/4 - \epsilon_p/4$ .

Finally, the Hamiltonian is transformed back into the original basis set of  $\{|s\rangle, |p_x\rangle, |p_y\rangle, |p_z\rangle\}$ . The final Hamiltonian block matrix for the surface atom becomes

$$\begin{bmatrix} \epsilon_s + \frac{\delta_{sp^3}}{2} & 0 & \frac{\delta_{sp^3}}{2} & 0 \\ 0 & \epsilon_p + \frac{\delta_{sp^3}}{2} & 0 & \frac{\delta_{sp^3}}{2} \\ \frac{\delta_{sp^3}}{2} & 0 & \epsilon_p + \frac{\delta_{sp^3}}{2} & 0 \\ 0 & \frac{\delta_{sp^3}}{2} & 0 & \epsilon_p + \frac{\delta_{sp^3}}{2} \end{bmatrix}. \quad (5)$$

In comparison with Eq. (2), this block matrix contains nonzero off-diagonal elements. Furthermore, the shift of the diagonal element is proportional to the number of dangling bonds. If the surface atom has  $n$  dangling bonds, the energy shift of the diagonal elements is given by  $n\delta_{sp^3}/4$ . This shows that BC II distinguishes among surface atoms with a different number of dangling bonds. It is important to note that BC II becomes identical to BC I when the energies of all the four  $sp^3$  hybridized orbitals are raised by the same amount. Therefore, BC I can be interpreted as the boundary condition that truncates the dangling bonds as well as the bonds connected to interior atoms.

To some degree, BC II mimics the physical passivation of dangling bonds with other atoms such as hydrogen and oxygen. Experimentally, silicon surfaces are usually passivated by hydrogen to improve the conductivity. The hydrogen forms bonding and anti-bonding states with the dangling bonds of Si at the surface. For example, the energies of the bonding and anti-bonding states of  $\text{SiH}_4$  are about 18 eV and 5 eV below the valence band edge of bulk Si, respectively.[7] Therefore, hydrogen passivation efficiently removes surface states localized in dangling bonds. In connection with this mechanism, BC II can be interpreted as the approximate formation of the bonding and antibonding states between a dangling bond and vacuum at an energy determined by  $\delta_{sp^3}$ . [8]

Although BC I and II can be also applied to excited orbitals such as  $d$  and  $s^*$ , it is unnecessary to shift the energies of the excited orbitals for surface atoms. The atomic energies of the excited orbitals (typically 10–20 eV) are larger than the energy gap, which is typically 0–5 eV.[9] Furthermore, the bonding states between the excited orbital and the  $s/p$  orbital are shifted up by the energy shift of the  $s/p$  orbitals. Therefore, the unmodified excited orbitals of surface atoms do not lead to surface states in the middle of the energy gap.

Implementing BC I and II requires a proper choice for the energy shift of the surface atoms. The energy shift should be high enough to discourage electrons from occupying the surface atom orbitals and consequently to eliminate all non-physical surface states in the middle of the gap. The diagonal elements of the tight-binding Hamiltonian give a guide to the required energy shift. The diagonal elements range from 0.6 eV to 20 eV. The sensitivity of the electronic structure to different energy shifts  $\delta_s$ ,  $\delta_p$ , and  $\delta_{sp^3}$  is discussed in Section IV D.

Finally for BC III (the periodic boundary condition), every surface atom is connected

with another surface atom on the opposite side of the supercell. Consequently, the coupling between surface atoms from the two sides is added to the original Hamiltonian:

$$H_{periodic} = H_0 + \sum_{\langle jk \rangle \gamma \gamma'} t_{jk\gamma\gamma'} |j, \gamma\rangle \langle k, \gamma'|, \quad (6)$$

where  $\langle jk \rangle$  denotes all the new pairs of neighbors due to the periodic boundary condition. The diagonal block matrix of the Hamiltonian for surface atoms is unchanged in the periodic boundary condition as opposed to BC I and II.

### III. NANOSTRUCTURE MODELING

The three boundary conditions are applied to the study of the electronic structure of a self-assembled InAs quantum dot embedded in a GaAs buffer. The modeled dot is lens shaped with diameter 15 nm and height 6 nm, similar to experimentally available dots.[10, 11]. The appropriate size for the GaAs buffer depends on the type of calculation. For strain-profile calculations, the buffer thickness should be at least as large as the dot size since the strain field is long-ranged, while for electronic-structure calculations the buffer thickness can be smaller than the dot size because bound electron states are effectively confined inside the dot.[4] In this work, a 15 nm thick buffer is used for the strain-profile calculation, and a reduced buffer with thickness 1 – 5 nm is used for the electronic structure calculation with the atomic positions given by the larger strain calculation. The equilibrium atomic positions are calculated by minimizing the strain energy using an atomistic valence-force-field model.[3, 12, 13] The necessity of a large buffer size for the strain calculation and the long-range effect of the strain on the electronic structure are discussed in Section IV A. Under the saturated strain profile obtained with a sufficiently large buffer, the quantitative effect of the reduced buffer size on the electronic structure is examined in Section IV E.

The tight-binding Hamiltonian for the InAs dot and the GaAs buffer is constructed based on atomic  $sp^3d^5s^*$  orbitals. The Hamiltonian matrix elements are obtained by fitting to experimental bulk band structure parameters with a genetic optimization algorithm.[3, 14] To take into account the effect of the displacements of atoms from the unstrained crystal positions, the atomic energies (the diagonal elements of the Hamiltonian) are adjusted by a linear correction within the Löwdin orthogonalization procedure.[14, 15] The coupling parameters between nearest-neighbor orbitals (the off-diagonal elements of the Hamiltonian)

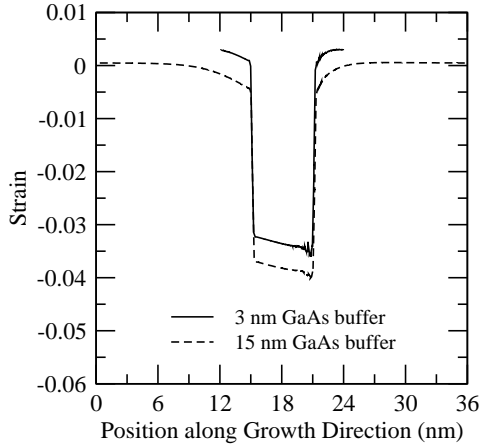


FIG. 1: Strain profiles for a lens-shaped InAs quantum dot with diameter 15 nm and height 6 nm, embedded in 3 nm and 15 nm thick GaAs buffers. The hydrostatic strain component  $(\epsilon_{xx} + \epsilon_{yy} + \epsilon_{zz})/3$  is plotted with respect to atomic position along the growth direction from the substrate to the capping layer. The periodic boundary condition is imposed on the buffer surface. The simulation with the small buffer underestimates the compressive strain inside the dot by 0.005 in comparison with the simulation with the large buffer. Furthermore, the small-buffer simulation predicts a tensile strain in the buffer while the large-buffer simulation predicts a compressive strain.

are also modified according to the generalized Harrison  $d^{-2}$  scaling law and Slater-Koster direction-cosine rules.[16, 17]

The eigenvalues of the tight-binding Hamiltonian is obtained with the Lanczos algorithm,[18] which is a commonly used iterative eigenvalue solver for large-dimensional, sparse, Hermitian matrices, as is the case for our tight-binding Hamiltonian. At each Lanczos iteration, the matrix is projected into a lower-dimensional subspace known as the Krylov subspace. The reduced matrix is tridiagonal and its eigenvalues approximate those of the original matrix as the size of the Krylov subspace grows.

## IV. RESULTS AND DISCUSSION

### A. Long-ranged Strain Field

An accurate strain profile is a prerequisite for the electronic-structure calculation because the strain field strongly affects ionic potentials and thus changes the electron Hamiltonian.



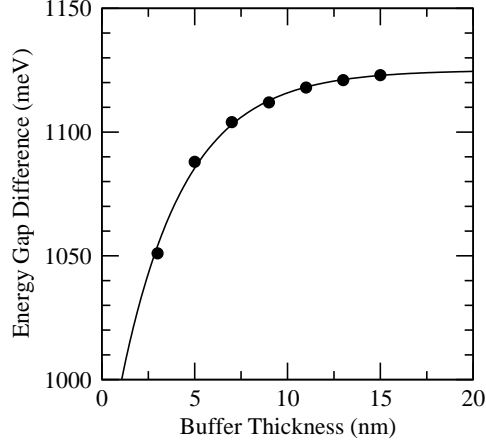


FIG. 2: Energy gap between the ground electron and hole states with respect to untruncated GaAs buffer thickness. The modeled system is an InAs dot with diameter 15 nm and height 6 nm, embedded in a GaAs buffer. Both strain profile and electronic structure are calculated with the periodic boundary condition imposed on an untruncated buffer surface. The solid circle is the calculation result, and the line is an exponential fit. As the buffer thickness increases and the strain in the dot saturates, the energy gap converges to 1.125 eV.

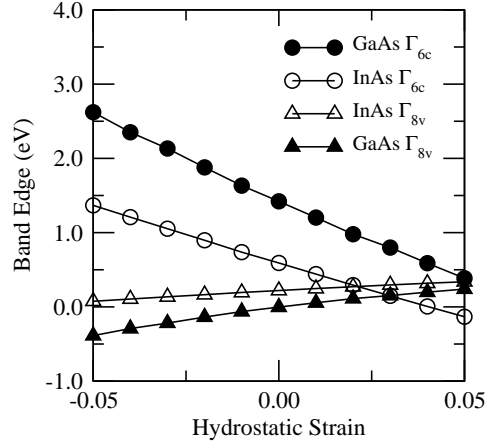


FIG. 3: Conduction and valence band edges at  $\Gamma$  with respect to hydrostatic strain for bulk InAs and GaAs. The compressive strain increases the direct band gap while the tensile strain decreases the gap.

In order to obtain an accurate strain profile of InAs/GaAs nanostructures, a sufficiently large GaAs buffer needs to be included in the simulation domain. Figure 1 shows the dramatic difference between the strain profiles calculated with a 3 nm thick buffer and a 15 nm thick buffer. The simulation with the small buffer underestimates the compressive strain inside

the dot and misrepresents the strain in the buffer. The simulation with the large buffer yields the relaxation of strain at the buffer surface. The result indicates that the 15 nm thick buffer is sufficiently large to accommodate the strain relaxation that would occur in a realistically sized system.

The saturation of the strain profile can be also monitored by examining the convergence of the resulting electronic structure. Figure 2 shows the energy gap between the ground electron and hole states with respect to the buffer size used for both strain and electronic structure calculations. Both the strain profile and the electronic structure are calculated with the periodic boundary condition. As the buffer thickness varies from 3 nm to 15 nm, the resulting energy gap increases by about 72 meV (from 1.051 eV to 1.123 eV). The large gap change demonstrates the long-range effect of the strain field on the electronic structure. The exponential fit suggests the convergence of the gap to 1.125 eV as the buffer thickness becomes infinite. Since the small buffer underestimates the strain inside the dot, the increase of the buffer thickness results in the increase of the dot strain. Under the compressive hydrostatic strain, the bulk GaAs and InAs conduction (valence) band edge at  $\Gamma$  shifts up (down), as shown in Figure 3. Following the trends, the lowest conduction (the highest valence) electron energy of the strained nanostructure increases (decreases) as the buffer thickness increases and the dot strain becomes stronger. These shifts of the electron energies lead to the overall increase of the energy gap. Figures 1 and 2 clearly demonstrate the importance of a sufficiently large buffer size in the simulation domain in order to obtain both accurate strain profile and electronic structure.

Although the strain calculation requires a large buffer, an accurate electronic structure can be obtained with a smaller buffer due to the finite extent of the localized electron wave functions. Using a truncated buffer will ease the computational requirements for the electronic structure calculation since the dimension of the Hamiltonian grows linearly with the number of atoms included in the model. From here on, the electronic structure is calculated with a truncated buffer while keeping the equilibrium atomic positions obtained from the strain calculation using a 15 nm thick buffer and implementing the boundary conditions addressed in Section II. The efficiency and reliability of each boundary condition are systematically analyzed in terms of the elimination of non-physical surface states in Section IV B, the number of Lanczos iterations required for interior-state energy convergence in Section IV C, the insensitivity of the converged energy to the boundary energy shift in

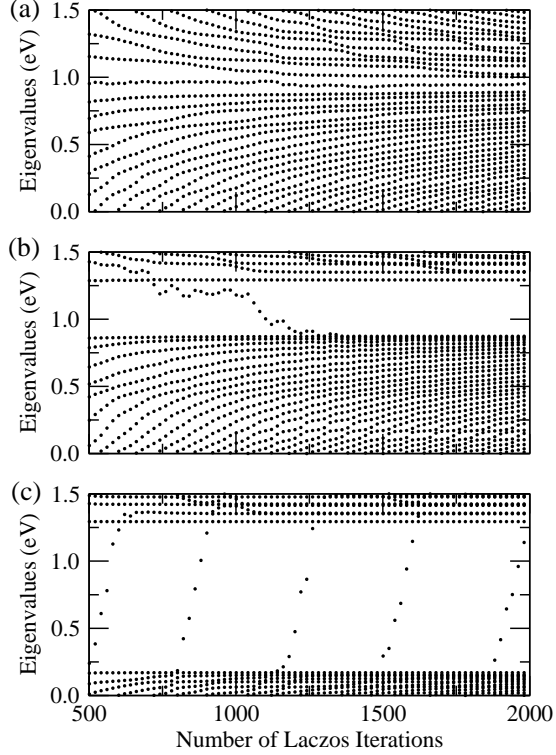


FIG. 4: Eigenvalues of the Lanczos tridiagonal matrix versus the number of Lanczos iterations (a) without any modification to boundary energies, (b) with the boundary condition of raising surface-atom orbital energies (BC I), and (c) with the boundary condition of raising dangling-bond energies (BC II). The modeled system is an InAs dot with diameter 15 nm and height 6 nm, embedded in GaAs. The strain is calculated with a 15 nm thick GaAs buffer, while the electronic structure is calculated with a truncated buffer with thickness 3 nm. The energy shifts for the boundary condition are set to be (b)  $\delta_s=5$  eV,  $\delta_p=3$  eV, and (c)  $\delta_{sp^3}=5$  eV.

Section IV D, and the buffer size required for the energy convergence in Section IV E.

## B. Surface/Interface State Elimination

One important criterion for a proper BC is the elimination of non-physical surface/interface states from the energy region of interest. Figure 4 presents the eigenvalues obtained from the Lanczos iterations when three different boundary conditions are applied to a 3 nm thick truncated buffer. First, to visualize the importance of having a proper boundary condition, the eigenvalues without any modification to the boundary energies are

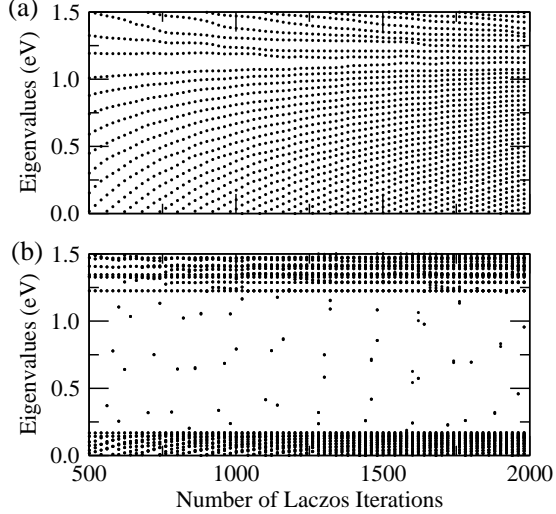


FIG. 5: Eigenvalues of the Lanczos tridiagonal matrix versus the number of Lanczos iterations with the periodic boundary condition (BC III) (a) using the truncated buffer with thickness 3 nm and (b) using the untruncated buffer with thickness 3 nm. The difference between the two buffers lies in the equilibrium positions of atoms, since the former buffer uses the result of the strain calculation with a 15 nm thick buffer while the latter buffer uses that with a 3 nm thick buffer. The strain profile results for the two cases are shown in Fig. 1.

plotted in Figure 4(a). When such a trivial boundary condition is implemented, many surface states are formed, which prevents the Lanczos algorithm from resolving eigenvalues for the physical interior states. By comparison, Figure 4(b) and (c) show that BC I and II remove surface states and develop an energy gap. The energy shifts used in this calculation are  $\delta_s=5$  eV,  $\delta_p=3$  eV, and  $\delta_{sp^3}=5$  eV. BC II efficiently eliminates all non-physical surface states in the middle of the gap between about 0.3 eV and 1.2 eV. In contrast, BC I does not remove all the surface states. The dense spectrum of the remaining surface states prevents the convergence of bound hole states below 0.3 eV.

BC III is also applied to the truncated buffer to test its efficiency in interface-state elimination. Figure 5 shows the eigenvalues of the Lanczos tridiagonal matrix with the periodic boundary condition: (a) using a truncated buffer with thickness 3 nm and (b) using an untruncated buffer with thickness 3 nm. In the former the strain profile is calculated with a 15 nm thick buffer and then the buffer is reduced to 3 nm to calculate the electronic structure, while in the latter both the strain profile and electronic structure are calculated with a 3 nm thick buffer. In both cases, the periodic boundary condition is imposed for not

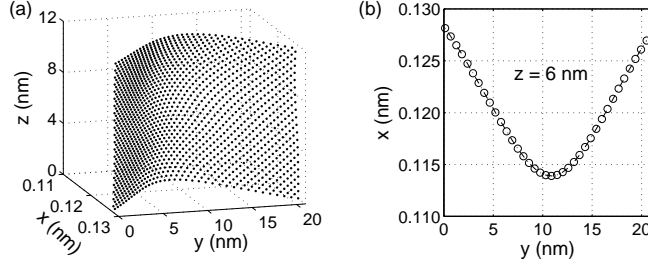


FIG. 6: Atomic positions at the boundary plane of the truncated GaAs buffer: (a) 3-D visualization of the boundary plane, (b) a slice through a plane with  $z$  about 6 nm. The plane is bent due to non-uniform strain generated by the lattice mismatch between the InAs dot and GaAs buffer. The variation of the atomic positions along the  $x$  axis is about 5% of the unstrained bond length of 0.24 nm.

only the electronic structure calculation but also the strain profile. The periodic boundary condition with the truncated buffer results in many spurious states in the middle of the gap, while that with the untruncated buffer does not.

The mid-gap states in the truncated-buffer simulation are formed because of the non-planar interface at the boundaries. A lattice mismatch of 7% between InAs and GaAs induces strain in both the InAs dot and the GaAs buffer. The strain bends the boundary plane of the truncated buffer by as much as 5% of the unstrained GaAs bond length (see Fig. 6). When the bent boundaries are connected by the periodic boundary condition, the bond between the atoms at the interface is significantly stretched or compressed. The strained bonds result in non-physical “interface” states in the middle of the gap. As shown in Figure 3, strain dramatically change the band structure of bulk GaAs — tensile strain reduces the band gap while compressive strain increases the gap. Similarly, the strongly strained interface in the truncated buffer yield mid-gap states. In contrast, the boundaries of the untruncated buffer are smooth due to the periodic boundary condition imposed on the strain calculation. As a result, it does not yield interface states. However, because of its inaccurate strain profile the resulting electronic structure is also inaccurate as discussed in Section IV A.

To avoid the unrealistic interface states induced by the truncated periodic BC, the atomic positions of the truncated buffer need to be adjusted to flatten the interface.[5] However, the adjustment unavoidably leads to an inaccurate strain profile unless the truncated buffer is

TABLE I: Number of Lanczos iterations required to obtain eigenvalues converged within  $0.1 \mu\text{eV}$  with the boundary condition of raising orbital energies of surface atoms (BC I) and with the boundary condition of raising dangling-bond energies (BC II). The modeled system is a lens-shaped InAs quantum dot with a diameter 15 nm and height 6 nm, embedded in a 3 nm thick GaAs buffer. The strain profile is obtained with a 15 nm thick GaAs buffer.

| No. of eigenvalues | BC I | BC II |
|--------------------|------|-------|
| 1                  | 1250 | 650   |
| 2                  | 2320 | 1370  |
| 3                  | 2400 | 1370  |
| 4                  | 2420 | 1370  |

large enough for strain to saturate near the interface. We have experimented with a partial relaxation of the boundary layers but found unsatisfactory results — many interface states remain, because the partial relaxation is not sufficient to flatten the interface. To succeed in eliminating interface states, one should start with a larger buffer whose boundary is less strained so that the partial relaxation can lead to a flat boundary.

BC I and II do not require any adjustment to the interface of the truncated buffer, as opposed to BC III which requires an artificial flattening of the interface. Therefore, we conclude that the non-periodic BCs are more efficient than the periodic BC in terms of the elimination of surface or interface states with a smaller truncated buffer while accurately incorporating the strain profile resulting from a larger-buffer simulation.

### C. Eigenvalue Convergence Speed

To investigate the efficiencies of BC I and II in resolving interior-state energies, the speed of the eigenvalue convergence is measured in terms of the number of Lanczos iterations required. Table I lists the number of Lanczos iterations required for a given number of converged eigenvalues for BC I and II. BC II results in a faster convergence than BC I. For example, to acquire four eigenvalues, BC II requires half as many iterations as BC I. The efficiency of BC II is attributed to the elimination of the dense spectrum of surface states. In general, iterative eigenvalue solvers easily find eigenvalues in a sparse spectrum, but show

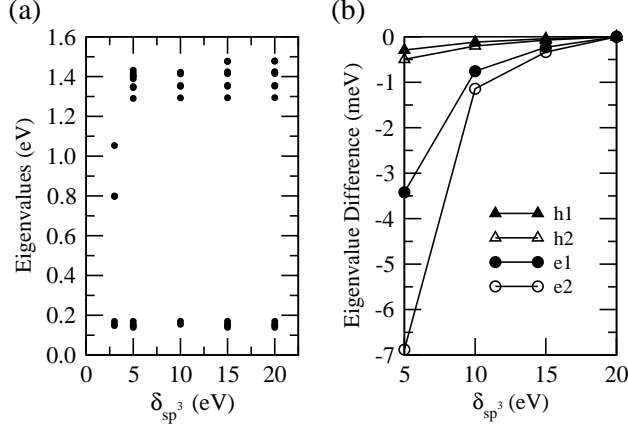


FIG. 7: (a) Electron energy versus dangling-bond energy shift  $\delta_{sp^3}$ , (b) Variations of the ground and excited electron (e1, e2) and hole (h1, h2) energies with respect to energy shift. A energy shift larger than 5 eV eliminates surface states in the middle of the gap between 0.2 and 1.2 eV. The electron and hole energies vary only by a few meV when the energy shift varies from 5 to 20 eV.

difficulty resolving eigenvalues in a dense spectrum. Therefore, the search of interior states is accelerated by the elimination of surface states from the interior-state spectrum.

#### D. Boundary Energy Shift

To implement BC I and II, appropriate boundary energy shifts  $\delta_s$ ,  $\delta_p$ , and  $\delta_{sp^3}$  must be determined. The ultimate goal in choosing the energy shift is to eliminate all surface states in the energy region of interest for interior states (e.g., within the band gap). Figure 7 shows converged eigenvalues with respect to the energy shift  $\delta_{sp^3}$  in BC II. While  $\delta_{sp^3}=3$  eV leads to surface states in the middle of the gap, the energy shift larger than 5 eV eliminates all the surface states and leads to the eigenvalues converged within a few meV. This indicates that the electronic structure is insensitive to the choice of the energy shift in BC II if the shift is big enough to remove all surface states.

In contrast, the effect of energy shifts on the electronic structure with BC I is highly unpredictable; a slight change of the shifts leads to a completely different Lanczos eigenvalue spectrum. For instance, changing  $\delta_p$  from 3 eV to 4 eV results in more surface states within the gap, as shown in Figure 8. A wide range of positive and negative energy shifts  $\delta_s$  and  $\delta_p$  was tested to achieve the best performance for eliminating surface states. However, no pair

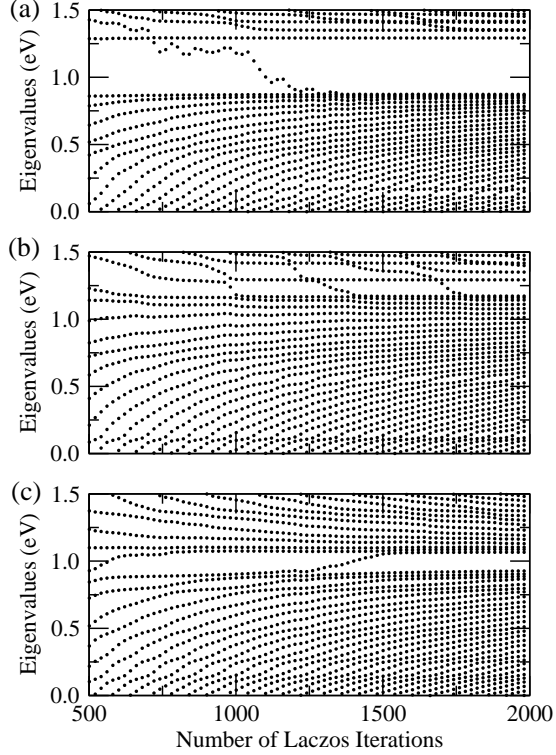


FIG. 8: Eigenvalues of the Lanczos tridiagonal matrix versus the number of Lanczos iterations with the boundary condition of raising orbital energies (BC I), (a) using  $\delta_s=5$  eV and  $\delta_p=3$  eV, (b) using  $\delta_s=5$  eV and  $\delta_p=4$  eV, and (c) using  $\delta_s=20$  eV and  $\delta_p=20$  eV. We have not found any pair of  $\delta_s$  and  $\delta_p$  that succeeds in removing all the surface states in the middle of the gap which is between 0.2 and 1.2 eV.

of tested  $\delta_s$  and  $\delta_p$  within 20 eV succeeded in eliminating all the surface states and in yielding the band gap 1.1 eV which is given by both BC II with a truncated buffer (see Fig. 4 (c)) and BC III with an untruncated buffer (see Fig. 5 (b)). This inefficiency in removing surface states is attributed to the truncation of connected bonds. BC I truncates both dangling bonds and connected bonds, while BC II truncates only the dangling bonds. Since the connected bond should be connected to interior atoms, the truncation of the connected bond will create a dangling bond to the interior atoms, and the dangling bond gives rise to surface states within the gap. This result suggests that BC I has intrinsic difficulties in removing surface states.



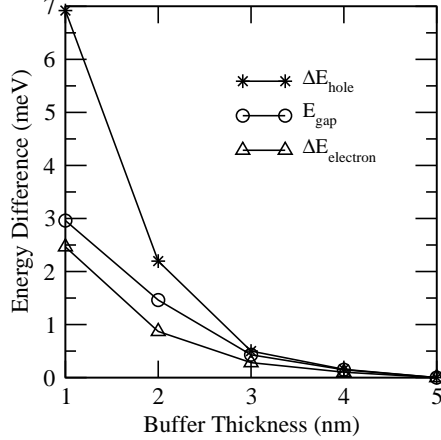


FIG. 9: Variations of the energy gap ( $E_{\text{gap}}$ ) between the ground electron and hole states, the energy spacing ( $\Delta E_{\text{electron}}$ ) between the ground and the first excited electron states, and the energy spacing ( $\Delta E_{\text{hole}}$ ) between the ground and the first excited hole states, with respect to the truncated buffer thickness for an InAs quantum dot with diameter 15 nm and height 6 nm. The boundary condition of raising dangling-bonds energies (BC II) with  $\delta_{sp^3}=10$  eV is used for this calculation.  $E_{\text{gap}}$ ,  $\Delta E_{\text{electron}}$ , and  $\Delta E_{\text{hole}}$  with each buffer thickness are subtracted by those with buffer thickness 5 nm to obtain the variations of these quantities. As the buffer thickness becomes larger than 3 nm,  $E_{\text{gap}}$ ,  $\Delta E_{\text{electron}}$ , and  $\Delta E_{\text{hole}}$  converge to 1123 meV, 56 meV, and 14 meV within 1 meV, respectively.

### E. Buffer Size

To find a reasonable buffer size for accurate electronic-structure calculations, the quantitative dependence of the electronic structure on the buffer size is examined. BC II is used since it provides the most efficient elimination of non-physical states. Figure 9 presents the energy gap between the lowest conduction electron and the highest valence electron levels for different buffer thicknesses. The buffer thickness is defined as the distance between the faces of the buffer GaAs box and the InAs dot. When the buffer thickness is bigger than 3 nm, the energy gap and the electron and hole energy spacings converge to 1123 meV, 56 meV, and 14 meV within 1 meV, respectively. This convergence indicates that a 3 nm thick buffer is large enough to obtain the electronic structure with the accuracy of 1 meV. In general, the optimal buffer size varies with quantum-dot size and electron level, and hence one should determine the optimal size by monitoring the convergence of the energies for a

desired accuracy.

## V. CONCLUSIONS

In summary, we have investigated three types of boundary conditions for the electronic structure of a self-assembled InAs dot embedded in GaAs within the framework of the empirical tight-binding model. Two non-periodic boundary conditions demonstrate higher efficiency than the truncated periodic boundary condition, in terms of the buffer size required to eliminate non-physical mid-gap states. Between the non-periodic boundary conditions, BC II (raising dangling-bond energies) more efficiently removes surface states than BC I (raising orbital energies of surface atoms). Therefore, BC II is identified as the most efficient boundary condition for eliminating surface states and achieving the convergence of interior-state energies with a truncated buffer.

The effect of the dangling-bond energy shift and the buffer size on the electronic structure have been further examined with the efficient BC II. An energy shift bigger than 5 eV efficiently removes all spurious states in the middle of the gap, and yields an energy gap insensitive to the further increase of the energy shift. For a lens-shaped InAs dot with diameter 15 nm and height 6 nm, the GaAs buffer thickness of 3 nm is large enough to obtain the electronic structure with the accuracy of 1 meV.

While our new boundary condition (BC II) has been developed within the framework of empirical tight binding, it can be extended to other models. An example is to use an empirical pseudo-potential with a non-local part that is a sum of projections on sub-spaces with well-defined orbital momentum.[19] In this case, a transformation of the basis set to the  $sp^3$  hybridized orbitals can be performed and an energy shift can be applied solely to the dangling bonds as presented in this work.

Boundary condition II with a truncated buffer takes advantage of the localization of the electron wave functions in a core nanostructure such as the InAs/GaAs quantum dot illustrated in this article. This scheme is not straightforwardly applicable to other types of heterostructures where electrons or holes are localized in the buffer. However, if the core nanostructure is larger than the extent of the electron or hole wave function localized in the buffer, one can truncate the core region instead of the buffer. When one of the carriers (electron or hole) is localized in the core and the other carrier in the buffer, the core carrier

can be modeled with a truncated buffer and the buffer carrier with a truncated core, so long as the coupling between the conduction and valence bands is weak enough to treat the electron and hole Hamiltonians independently.

### Acknowledgments

This work was performed at Jet Propulsion Laboratory, California Institute of Technology under a contract with the National Aeronautics and Space Administration. This work was supported by grants from NSA/ARDA, ONR, and JPL internal Research and Development.

- 
- [1] G. Klimeck, R. K. Lake, R. C. Bowen, W. R. Frensley, and T. Moise, *Appl. Phys. Lett.* **67**, 2539 (1995).
  - [2] D. Mamaluy, M. Sabathil, and P. Vogl, *J. Appl. Phys.* **93**, 4628 (2003).
  - [3] G. Klimeck, F. Oyafuso, T. B. Boyking, R. C. Bowen, and P. von Allmen, *Computer Modeling in Engineering and Science* **3**, 601 (2002).
  - [4] F. Oyafuso, G. Klimeck, P. von Allmen, and T. B. Boykin, *Phys. Status Solidi B* **239**, 71 (2003).
  - [5] L.-W. Wang, J. Kim, and A. Zunger, *Phys. Rev. B* **59**, 5678 (1999).
  - [6] When a system is under non-hydrostatic strain, the bond directions are different from those in an unstrained structure. However, the difference is small enough to ignore in the modeled system, where the maximum strain is about 5%. Therefore, we use *sp* hybridized orbitals that are aligned along the bond directions of the unstrained structure.
  - [7] M. Cardona, *Phys. Status Solidi B* **118**, 463 (1983).
  - [8] The explicit modeling of surface passivation would lead to a larger Hamiltonian dimension and consequently more computation time than BC II due to the passivation atoms.
  - [9] J.-M. Jancu, R. Scholz, F. Beltram, and F. Bassani, *Phys. Rev. B* **57**, 6493 (1998).
  - [10] K. H. Schmidt, G. Medeiros-Ribeiro, J. Garcia, and P. M. Petroff, *Appl. Phys. Lett.* **70**, 1727 (1997).
  - [11] J. M. Garcia, G. Medeiros-Ribeiro, K. Schmidt, T. Ngo, J. L. Feng, A. Lorke, J. Kotthaus, and P. M. Petroff, *Appl. Phys. Lett.* **71**, 2014 (1997).

- [12] P. Keating, Phys. Rev. **145**, 637 (1966).
- [13] C. Pryor, J. Kim, L. W. Wang, A. J. Williamson, and A. Zunger, J. of Appl. Phys. **83**, 2548 (1998).
- [14] T. B. Boykin, G. Klimeck, R. C. Bowen, and F. Oyafuso, Phys. Rev. B **66**, 125207 (2002).
- [15] P.-O. Löwdin, J. Chem. Phys. **18**, 365 (1950).
- [16] W. A. Harrison, *Elementary Electronic Structure* (World Scientific, New Jersey, 1999).
- [17] J. C. Slater and G. F. Koster, Phys. Rev. **94**, 1498 (1954).
- [18] L. N. Trefethen and D. B. III, *Numerical Linear Algebra* (Society for Industrial and Applied Mathematics, Philadelphia, 1997), pp. 276–284.
- [19] A. J. Williamson, L.-W. Wang, and A. Zunger, Phys. Rev. B **62**, 12963 (2000).